Universiteit Leiden
The Netherlands

Anyonic, cosmic, and chaotic: three faces of Majorana fermions
Cheipesh, Y.I.

Chapter 1

Introduction

1.1 Preface

This thesis is devoted to the study of a model that finds useful and important applications in a wide range of physical systems, from cosmology and particle physics to condensed matter physics and quantum computers. It tries to support the idea that working on the intersection of different fields of physics is extremely fruitful and that studying low energy effective field theories can give us a lot of insight about high energy fundamental theories.

The state of the art of modern physics describes matter as consisting of fermionic particles that interact through bosonic mediators (with the Higgs boson playing yet another special role). Attempts to build a closed, complete and self-consistent quantum mechanical description of atomic and sub-atomic physics started at the beginning of 20th century and culminated in the so-called Standard Model [1]. At the moment, it describes a zoo of all particles that have been detected so far. These particles have many interesting and peculiar properties such as chiral interactions, non-abeliean symmetries, etc. To study them, particle physicists build larger and larger facilities such as accelerators, colliders, gigantic detectors.

A complementary avenue to study the properties of the particles on low energy scales is provided by condensed matter physics. Both at the high- (particle physics) and low-energy end (condensed matter physics), physics is of irreducible emergent many-particle nature and it is only in the middle (atomic and nuclear physics) that few-particle systems come into play. Collective degrees of freedom of a many-body system can be described by so-called "quasi particles" [2]. Such many-body systems are governed by qual-

itatively new principles (also called "laws of emergent behaviours"), compared to few-particle systems [3].

The properties of these quasi-particles such as statistic, charge, effective mass, etc. are typically defined not by the microscopic details, but by the universal properties of the system, *e.g.* its symmetries. Modern technologies allow to fabricate complex many-body systems that can host quasi particles with predefined properties, which can be probed experimentally. On the other hand, the principle of adiabatic continuity allows us to study such systems theoretically. One can forget about microscopic details and consider simpler "toy" effective models with specified symmetries [3].

One interesting and yet not fully studied example are the so-called Majorana fermions – neutral particles with fermionic (or, in general, anyonic) statistics that have a peculiar property: they can be considered as their own anti-particles [4]. Although no elementary particles has so far been confirmed to be a Majorana fermion, they play a very important role both in fundamental and applied physics. From the point of the former, there are several reasons to consider Majorana fermions:

1. ordinary Standard Model neutrinos may appear to be Majorana fermions. This possibility is being tested in, *e.g.*, experiments of the so-called neutrino-less double β decay [5–7].

2. despite the great experimental success of the Standard Model, which has been verified to a high precision in thousands of different channels, we know for sure that it is incomplete. This means that there should exist some new particles. Majorana fermions could be a very good candidate for several reasons:

   (a) Majorana fermions have been proposed as a dark matter particle (*e.g.* WIMPs, sterile neutrinos) [8–10].
   (b) a Majorana lepton breaks lepton number conservation. This is the key element of the so-called thermal leptogenesis – one of the most popular mechanisms for the explanation of the matter-antimatter asymmetry [11, 12].
   (c) the Majorana mass of right-handed neutrinos provides a very natural explanation of the minuteness of normal neutrino masses (seesaw mechanism) [13].

We do not know what is the correct extension of the Standard Model. Even if Majoranas are not the right candidates and do not exist in nature as

a fundamental particle, we are still left with a lot of motivation to study them from the perspective of mesoscopic physics, where they can be constructed out of electron and hole excitations [14–16].

Recently, there has been a lot of attention to so-called *Majorana zero modes* (MZMs) – subgap states in superconductors [16–19]. There they arise as a quasiparticle excitation localized at the boundaries. Such MZMs are spatially separated, pinned to have exactly zero energy and free of decoherence thanks to the particle-hole symmetry of the superconducting state. Moreover, unlike ordinary fermions and bosons, they have a non-abelian anyonic statistics under the exchange. Thanks to these properties one can use them as building blocks for a protected quantum memory [17, 20, 21] for a fault-tolerant quantum computer.

The effective low energy field theory of the MZMs in superconductors is a non-interacting theory. A very interesting physics emerges also if one looks at a different end - strongly interacting Majorana modes in the many-body systems. If one couples $N \gg 1$ such modes in a way that the coupling is all-to-all and random [22, 23], the resulting system would have a non-Fermi liquid phase, where there is no clear Fermi surface even at zero temperature and the description of the system in terms of quasiparticles is not possible [24]. The theoretical toy model for such system is called Sachdev-Ye-Kitaev (SYK) model [25, 26] and it appears to be theoretically solvable under the mean-field approximation. It can be fruitful to study this toy model since there is still a need in the development of a general theory of the non-Fermi liquid ground state(s) of an interacting many-body fermionic system [24] and there are hints that SYK is capable of describing them to some extent. For example, the SYK model can reproduce some aspects of certain strongly correlated materials called strange metals [27]. Moreover, such a toy model has an emergent conformal symmetry in the infrared and saturates the upper bound on quantum chaos [28]. These aspects led to considering the SYK model to be a holographic dual of black hole horizons [29–31].

The points mentioned above are only a small part of the extensive list of arguments that make Majorana fermions an extremely interesting and rich subject of study.

1.2 Majorana fermions as fundamental particles

We start our investigation by looking at how the Majorana fermions emerge as elementary particles - real solutions of the fundamental Dirac equation [4].

1.2.1   Dirac equation

The first attempt to write a relativistic version of the Schrödinger equation $i\hbar\partial_t \ket{\psi} = \frac{\hat{p}^2}{2m}\ket{\psi}$ was made by Oskar Klein and Walter Gordon in 1926 by following the same logic of exploiting the dispersion relation, but in the relativistic form $E = \sqrt{p^2c^2 + m^2c^4}$ [32, 33]. However, such operator would be non-local, which is incompatible with the finite speed of light propagation. To get the local equation one needs to take the square of the dispersion relation, arriving to the famous Klein-Gordon equation $\left(\Box + \left(\frac{mc}{\hbar}\right)^2\right)\psi = 0$, where $\Box = g^{\mu\nu}\partial_\mu\partial_\nu = \frac{1}{c^2}\partial_t^2 - \nabla^2$ is a Lorentz-invariant combination.

However, the total probability $P = \int \mathrm{d}\vec{r}\,|\psi(\vec{r},t)|^2$, that used to be positive definite and conserved in time for the states obeying Schrödinger equation, loses its probabilistic interpretation in the Klein-Gordon equation, since we have also included the negative energy states when we took the square of $E(p)$. Indeed, the zeroth component of the conserved current $J_\mu \sim \psi^*\partial_\mu\psi - \psi\partial_\mu\psi^*$ can not be treated as the probability density since $J_0 = -\frac{\hbar|\psi|^2}{mc^2}\frac{\partial\arg(\psi)}{\partial t}$ can change sign.[1]

An alternative equation, proposed by Dirac in 1928, had the form of $i\hbar\partial_t\ket{\psi} = \hat{H}\ket{\psi}$ with $\hat{H} = \boldsymbol{\alpha}\cdot\hat{\mathbf{p}} + \beta m$ [32, 34]. In this case the probabilistic interpretation occurs automatically as the probability density is conserved for such equation with any Hermitian $\hat{H}$. Let us first consider the case of zero mass $m = 0$. Then, it can be shown that α_i do not commute, but rather satisfy $\{\alpha_i, \alpha_j\} = 2\delta_j^i$ which means that they are not numbers but matrices. One can also show that these matrices should be Hermitian, even-dimensional, traceless and that their eigenvalues are ± 1. The minimal set that satisfies these conditions are Pauli matrices $\sigma_{x,y,z}$ and the corresponding form of the Dirac equation is called *Weyl equation* $i\sigma^\mu\partial_\mu\ket{\psi} = 0$ [2]. Let us call *right spinor* ψ_R the 2-component wave function $\psi = (\psi_1, \psi_2)$ that is the solution of the corresponding Weyl equation. However, one can see that there is also another choice of $\alpha^i = -\sigma^i$ compatible with all the constraints that leads to the Weyl equation on left spinor $i\bar{\sigma}^\mu\partial_\mu\psi_L = 0$, where $\bar{\sigma}^\mu = (1, -\sigma^i)$. The names left and right come from the fact that one spinor relates to another through a parity transformation $P : \mathbf{r} \to -\mathbf{r}$ such that $\psi_L = \hat{P}\psi_R$.

Now let us try to introduce the mass into this equation. An important ob-

---

The contents of this chapter is mostly based on textbook material, for example one can follow the references [32]

[1] Klein-Gordon equation is, in essence, classical equation.

[2] Where we introduced the 4-vector $\sigma^\mu = (1, \sigma^i)$.

servation in this regard is that in order for the theory to be Lorentz-covariant, namely $i\sigma^\mu \partial'_\mu \psi'_R = i\sigma^\mu \Lambda^\mu_\nu \partial^\nu S_R \psi_R = S\left(i\sigma^\mu \partial_\mu \psi_R\right) = 0$ [3] (and the same holds for ψ_L but with some other matrices $S_L, \tilde{S}$), one has to require $S = S_L$ and $\tilde{S} = S_R$. In other words, the equation for he right spinor transforms as the left spinor and vice versa. This leads to the fact that the mass would mix right and left spinors since it is the only Lorentz-covariant way to introduce it

$$\begin{cases} i\sigma_\mu \partial^\mu \psi_R = m\psi_L \\ i\bar{\sigma}_\mu \partial^\mu \psi_L = m\psi_R \end{cases}. \tag{1.1}$$

Introducing the *Dirac spinor* $\Psi^T = (\psi_L, \psi_R)$ and the matrices $\gamma^\mu = \begin{pmatrix} 0 & \sigma^\mu \\ \bar{\sigma}^\mu & 0 \end{pmatrix}$, equations 1.1 become

$$\left(i\gamma_\mu \partial^\mu - m\right)\Psi = 0. \tag{1.2}$$

This representation of γ-matrices is not unique and is called *Weyl representation*.

Since the Hamiltonian of the Dirac equation commutes with p^μ the solutions are of a plane wave form with some spinor structure $\Psi(x) = u(p)e^{-ip^\mu x_\mu}$. By plugging it in the equation 1.2 and requiring to have a non-trivial solution for $u(p)$ we arrive at the constraint on the two solutions: $E = \pm\sqrt{\mathbf{p}^2 + m^2}$. Therefore, the general solution to the Dirac equation takes form $\Psi(x) = u(p)e^{-ip^\mu x_\mu} + v(p)e^{+ip^\mu x_\mu}$, where the spinors $u(p), v(p)$ have the interpretation of the particle and anti-particle.

The particle/antiparticle nature of the two solutions to the Dirac equation can be seen if one tries to build the positive energy counter-part ψ_c to the negative energy solution $\psi = v(p)e^{ip^\mu x_\mu}$. One can convince themselves that simple complex conjugation will not work and one should instead take $\psi_c = \hat{C}\psi^*$, where $\hat{C} = i\gamma^2$. Only in this case the opposite energy states ψ and ψ_c simultaneously solve Dirac equation. Physically, $\hat{C}$ is the operator of the charge conjugation, since in the presence of the electromagnetic field ψ_c satisfies the equation $\left(i\gamma^\mu(\partial_\mu + eA_\mu) - m\right)\psi_c = 0$, while for ψ the charge is opposite. This interpretation of the negative energy states comes very handy as it saves us from the catastrophe of the infinite negative energy sea of states (so-called Dirac sea).

---

[3] Where Λ^μ_ν is a boost matrix.

1.2.2   Majorana solution

In 1937, before disappearing, Majorana posed the question of whether we could look for a real solution to the Dirac equation [4]. This would be possible if one imposed the following constraint on the γ matrices present in the Dirac equation: $(i\hat{\gamma}^\mu)^* = i\hat{\gamma}^\mu$ (Majorana representation)[4]. Since the charge conjugation operator is generally chosen such that $-\hat{\gamma}^\mu \hat{C} = \hat{C}(\hat{\gamma}^\mu)^*$, for Majorana representation it commutes with γ-matrices and therefore the Majorana solutions are also eigenstates of the charge conjugation operator. In other words, the Majorana particle is electrically neutral and hence its own antiparticle $\Psi_c \equiv \hat{C}\Psi = \Psi$. The latter relation is what defines a Majorana particle in any representation and is called *Majorana condition*.

The Majorana solution can be written both in terms of a real four-component spinor, and as a complex two-component spinor. The equation on this two-component spinor can be understood from the following consideration. The charge conjugation operator in the Majorana representation is just a complex conjugation. This means that it changes the momentum of the state, but not the spin. For the massless case it would mean that the charge conjugation operator transforms the left spinor into the right[5], namely $\chi^c_{L/R} = \chi_{R/L}$. The Majorana spinor χ satisfies the equation

$$i\sigma^\mu \partial_\mu \chi - m\chi^c = 0. \tag{1.3}$$

1.3   Majorana fermions in condensed matter physics

Now when we are familiar with the Majorana fermions on the fundamental level, let us see how these (quasi)particles emerge in many-body condensed matter systems as effective low-energy degrees of freedom. The connection of the effective description of the low energy modes in many-body systems with the fundamental equations is very frequent with the most obvious example being graphene [35], followed by Weyl semimetals [36], etc. This should not be surprising, as the theory on low energies does not "see" the microscopic structure of the material, only its global symmetries.

---

[4]We note that the solutions *can* be real, but they do not need to, same as for the case of Klein-Gordon or Maxwell equations

[5]Dirac Hamiltonian commutes with the so-called helicity operator $\hat{h} = \hat{p} \cdot \hat{\Sigma}/|p|$. When $m = 0$, γ_5 also commutes with H and therefore the eigenstates have both fixed helicity and parity.

1.3.1 The need in superconductivity

Majorana fermions may or may not exist in Nature as elementary building blocks, but in condensed matter they can be constructed out of electron and hole excitations. In order to get the excitation that is charge neutral one needs superconductivity where the quasiparticles are coherent superpositions of electrons and holes – so-called *Bogoliubov quasiparticles*.

The mean-field Bardeen–Cooper–Schrieffer (BCS) Hamiltonian [37, 38] describing the conventional s-wave (the meaning of it will be elaborated further) superconductor is quadratic but includes so-called anomalous terms

$$H_{\text{BCS}} = \sum_{\mathbf{k}} \left[(\varepsilon_k - \mu)(c^\dagger_{\mathbf{k},\uparrow} c_{\mathbf{k},\uparrow} + c^\dagger_{-\mathbf{k},\downarrow} c_{-\mathbf{k},\downarrow}) + \Delta^* c_{-\mathbf{k},\downarrow} c_{\mathbf{k},\uparrow} + \Delta c^\dagger_{\mathbf{k},\uparrow} c^\dagger_{-\mathbf{k},\downarrow} \right],$$
(1.4)

where $\Delta = \frac{g_0}{V} \sum_{\mathbf{k}} \langle c_{-\mathbf{k},\downarrow} c_{\mathbf{k},\uparrow} \rangle$, V is a system volume and g_0 is some positive interaction constant.

Such kind of Hamiltonians are known to be diagonalized by the so-called Bogoliubov transformation which is in essence a rotation in the particle-hole space

$$\gamma^\dagger_{\mathbf{k},1} = u_{\mathbf{k}} c^\dagger_{\mathbf{k},\uparrow} + v_{\mathbf{k}} c_{-\mathbf{k},\downarrow}$$
$$\gamma_{-\mathbf{k},2} = v^*_{\mathbf{k}} c^\dagger_{\mathbf{k},\uparrow} - u^*_{\mathbf{k}} c_{-\mathbf{k},\downarrow}$$
(1.5)

with the condition that $u^2_{\mathbf{k}} + v^2_{\mathbf{k}} = 1$ and canonical commutation relations on quasiparticles $\{\gamma_{\mathbf{k},\alpha}, \gamma^\dagger_{\mathbf{k}',\beta}\} = \delta_{\mathbf{k},\mathbf{k}'} \delta_{\alpha,\beta}$. The Hamiltonian becomes diagonal $H_{\text{BCS}} = \sum_{\mathbf{k}} E_{\mathbf{k}} \left(\gamma^\dagger_{\mathbf{k},1} \gamma_{\mathbf{k},1} + \gamma^\dagger_{\mathbf{k},2} \gamma_{\mathbf{k},2} \right) + E_0$ with the eigenvalues

$$E_{\mathbf{k}} = \sqrt{(\varepsilon_{\mathbf{k}} - \mu)^2 + |\Delta|^2}$$
(1.6)

We can view $\gamma_{-k,2}$ as a creation operator of the particle with the negative energy and then the spectrum would look symmetric around $E = 0$. This means that the system has particle-hole symmetry – each eigenfunction Ψ at energy $E > 0$ has a copy $\Psi' = \hat{C}\Psi$ at energy $-E$, where $\hat{C}$ is a charge conjugation operator. Only at zero energy the particle and antiparticle can coincide which means that despite the fact that the quasiparticle excitations are coherent superposition of the particle and hole, we can not have Majorana quasiparticles in such a system because it would mean that we need to close the energy gap. Naively, if we allow for the superconducting gap Δ to become

k-dependent this obstacle can be bypassed and we can close the gap[6].

Let us consider a more general case where the Cooper pairing correlation (gap parameter) is a k-dependent tensor $\Delta_{\alpha\beta}(\mathbf{k}) \propto \langle c_\alpha(\mathbf{k}) c_\beta(-\mathbf{k}) \rangle$ with α, β being the spin indices. When there is no spin-orbit coupling, both the spin and the momentum are good quantum numbers, and one can separate $\Delta_{\alpha\beta}(\mathbf{k}) = \chi_{\alpha\beta}\Delta(\mathbf{k})$ with $\chi_{\alpha\beta}$ a spinor matrix and $\Delta(\mathbf{k})$ a function. Then, there are two possibilities:

1. $\chi_{\alpha\beta} = -\chi_{\beta\alpha}, \Delta(\mathbf{k}) = \Delta(-\mathbf{k})$ – the spin-singlet pairing.

2. $\chi_{\alpha\beta} = \chi_{\beta\alpha}, \Delta(\mathbf{k}) = -\Delta(-\mathbf{k})$ – the spin-triplet pairing.

One can write a general form of the order parameter as

$$\Delta_{\alpha\beta}(\mathbf{k}) = \left(\Delta_0(\mathbf{k}) + \mathbf{d}(\mathbf{k}) \cdot \sigma\right)(i\sigma_2)_{\alpha\beta}, \tag{1.7}$$

where $\Delta_0(\mathbf{k})$ encodes the singlet component and $\mathbf{d}(\mathbf{k})$ is a vector encoding the triplet state. Their functional dependence is generally unknown and depends on the particular lattice under consideration.

1.3.2 Topologically protected zero modes

If we do not have translational invariance in the system namely we have a system with an edge or a defect and if on top of that we also break the spin conservation, we can build Bogoliubov quasiparticle out of the creation and annihilation operator of the same mode [17, 39]

$$\begin{aligned} \gamma_{n1} &= c_n + c_n^\dagger \\ \gamma_{n2} &= i(c_n - c_n^\dagger). \end{aligned} \tag{1.8}$$

One can also think about it as simply a change of the basis where we double the degrees of freedom going to real modes – *Majorana representation*. For the systems with particle-hole symmetry we have a requirement that such states come in pairs at $\pm E$ with the possibility of an unpaired state at $E = 0$. The simplest example of the appearance of such a Majorana zero modes (MZM) is in the toy model called Kitaev chain [17]. There, the two MZMs are localized at the ends of the fermion chain.

Thanks to the particle-hole symmetry, the state at $E = 0$ is protected against any local perturbation that does not break particle-hole symmetry –

---

[6]Due to the symmetry of the spectrum with respect to $\vec{k} \to -\vec{k}$ this would be at the $k = 0$ or $k = \pm\pi$ points.

it simply is not able to shift from zero since the spectrum should be symmetric [15]. Such state is called *topologically protected*. One can also think about it as following - the Hamiltonian that has particle-hole symmetry commutes with the parity operator which means that different parity sectors are decoupled. The presence or absence of the zero energy state correspond to parity odd sectors. The only way for such state to disappear would be to bring the two Majorana modes that encode it close to each other such that their wave functions overlap. In this case the ground state will split and no longer be degenerate. For the example of the Kitaev chain it means that if the chain has finite length L then the state with MZMs at the end of the wire will have the energy of order $\varepsilon \sim e^{-L}$ instead of zero.

The presence or absence of the unpaired zero energy level is therefore in one-to-one mapping with the parity of the ground state that is a topological invariant protected by the particle-hole symmetry. Kitaev identified this invariant to be defined by the Pfaffian of the Hamiltonian in the basis of Majorana fermions $H = \frac{1}{2}\gamma \cdot \mathcal{A} \cdot \gamma, \mathcal{P}_0 = \mathrm{signPf}(-i\mathcal{A})$[7] [17]. The transition involving the change of the sign of the Pfaffian should necessarily involve closing of the gap.

It appears, that such topologically protected MZMs can appear not only in the toy models, but rather in real materials. We can depart from the superconductor with the presence of a defect or a boundary and see which additional constraints we have to impose. The first important ingredient to this story is that the zero energy level should be non-degenerate otherwise the two states at $E = 0$ can merge as $|11\rangle \to |00\rangle$[8]. This process is not forbidden in the superconductor since the latter only preserves the parity, not the particle number. It is known that the half-integer states in the system that has time reversal symmetry are doubly degenerate – so-called Kramers degeneracy [40]. The time-reversal operator changes both the direction of the spin and momentum. The two possible ways to break it are:

1. Take a *p*-wave superconductor with $\Delta_{\alpha\beta}(\mathbf{k}) \propto \begin{pmatrix} 1 & 0 \\ 0 & 0 \end{pmatrix} (k_x + ik_y)$ [15, 18, 41]. Such superconductors are called unconventional which reflects the fact that they are extremely rare in nature. Moreover, *p*-wave pairing is fragile, easily destroyed by disorder.

---

[7]The fact that the Hamiltonian can be represented as $H = i\mathcal{A}$, where $\mathcal{A}$ is a real antisymmetric matrix follows from the particle-hole symmetry which is just $H^* = -H$ in Majorana basis.

[8]Here we denote by $|1\rangle$ the presence of the state at zero energy.

2. A much simpler solution is to introduce the magnetic field that would break the time-reversal symmetry. Since the magnetic field is repelled from the superconductor (Meissner effect) and can only penetrate it in the form of vortices, we introduce superconductivity by proximitizing the semi-conductor with the superconductor. We take the *s*-wave superconductor since most superconductors in nature are of this kind. A singlet superconductor, however, has an important property: the total spin of every excitation is conserved. Zeeman field conserves the spin in *z*-direction, so together every single state of our system has to have a definite spin, including the Majoranas. Majoranas are their own particle-hole partners, and that means that they cannot have any spin (energy, charge, or any other observable property at all). This would mean that in such a system they can not appear. Therefore, the spin conservation needs to be broken and the simplest plausible way to do so is via the spin-orbit coupling (also referred to as Rashba coupling).

To conclude this analysis, in the system that consists of the semi-conductor, proximitized by the s-wave superconductor, with magnetic field and spin-orbit coupling one can have Majorana zero modes bound to a defect or a boundary that are spatially separated and protected from the local perturbations. Indeed, it happens so that by varying the strength of the magnetic field, chemical potential and superconducting gap one can close the gap in the energy spectrum and reopen it entering the so-called topological phase with the protected zero energy level.

There exist many proposals for the experimental realization of the topologically protected Majorana zero modes including chiral p-wave superconductors [42, 43], topological insulators in the proximity to the s-wave superconductor [16], semiconductors with Rashba spin-orbit coupling [19, 44, 45] (see Fig. 1.1).

1.3.3   Andreev levels

As was discussed above, the spectrum of the ideal topological superconductor under the mean field approximation is gapped (the gap being the mean field order parameter), so the zero energy level (if present) is well separated from the continuum. But is it still same for the "dirty" system with some disorder? The tool that can describe universal properties of disordered metals and superconductors [46, 47] depending on the symmetry class that it belongs to [48] is called Random matrix theory (RMT). The main idea is that instead
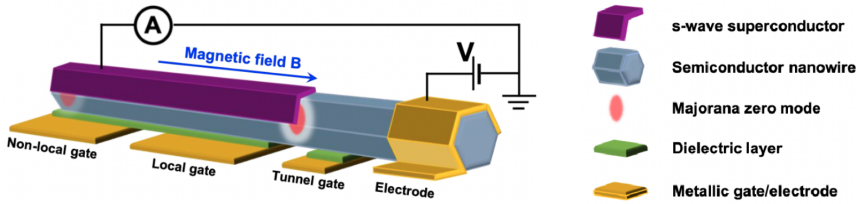
Figure 1.1. Schematic experimental setup of Majorana nanowire device. *The figure is reprinted with permission from Zhang, Hao, Dong E. Liu, Michael Wimmer, and Leo P. Kouwenhoven, Nature communications 10, no. 1, (2019)*

of considering one "ideal" Hamiltonian we take an ensemble of the Hamiltonians with some probability distribution $P(H) \sim \exp\left(-\frac{c}{N}\mathrm{Tr}H^2\right)$ where c is a parameter that is the same for the classes of Hamiltonians that share same universal symmetries [46].

When classifying the Hamiltonian classes we look only on anti-unitary symmetries that come in two types: the Hamitonian can either commute (time-reversal symmetry) or anti-commute (particle-hole symmetry) with the anti-unitary operator. All the unitary symmetries can be disregarded by restricting ourselves to one symmetry sector (block in the Hamiltonian matrix) and the unitary symmetry that anti-commutes with the Hamiltonian (called chiral symmetry) can be obtained as a product of particle-hole and time-reversal operators [49]. According to this, different combinations of these "non-reducible" symmetries give us 10 different classes of Hamiltonians [48] (corresponding to all the possible combinations of the symmetries).

In case of the systems that can host topologically protected Majorana zero modes, the spin-rotation symmetry is broken by spin-orbit coupling, while the particle-hole symmetry is present. The corresponding systems are in symmetry class D.

If one looks at the ensemble-averaged density of states for the class D system (Fig. 1.2), one would see that in the topologically non-trivial phase (green color and red delta-function contribution) there is a clear zero energy mode (corresponding to MZMs) that is well separated from the continuum – there is a dip in the density of states around zero. However, despite the fact that there is no sharp line at $E = 0$ for the topologically trivial case, the density of states is still peaked around zero [48, 50, 51].

This posses a fundamental obstacle on the route to measuring topologically protected zero modes since the accidentally low lying states (also called Andreev levels) in the trivial phase can mimic the true MZMs in the observables.
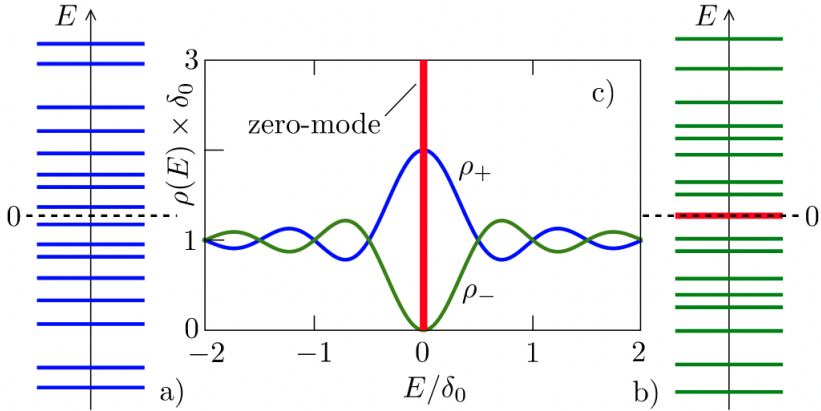
Figure 1.2. Panels a) and b) show the spectrum of a class-D superconductor. The unpaired MZMs are present on panel b). In the middle: the ensemble-averaged density of states. The green line and the delta-function contribution from the zero-mode correspond to the topological phase, while the blue line - to the trivial phase. *The figure is reprinted with permission from Beenakker, C. W. J, Reviews of Modern Physics, 2015*

The particular case when the observable is the parity of the sub-system of the system with $2N$ MaZMs is considered in Chapter 1.7.1 and Chapter 1.7.2.

1.4   Anyonic Majorana fermions

By definition, Majorana zero modes (MZMs) are real ($\gamma_i^\dagger = \gamma_i$) so we need two of them to encode a single complex fermion (each Majorana is an equal-weight superposition of the electron and hole excitation, Eq. 1.8). Moreover, in case of the topologically protected MZMs bound to defects or at the boundaries, such a fermion is de-localized.

For N zero energy levels we have $2N$ Majoranas and the degeneracy of the ground state is 2^N. The degeneracy of the ground state is a key element to the most valuable property of the topological superconductors - the non-Abelian statistic of the MZMs under the adiabatic exchange between one another

$$|\Psi\rangle \rightarrow \hat{U}|\Psi\rangle, \quad \text{where } U_{nm} = \exp\left(\pm\frac{\pi}{4}\gamma_n\gamma_m\right) = \frac{1}{\sqrt{2}}\left(1 \pm \gamma_n\gamma_m\right). \quad (1.9)$$

Such exchange of two MZMs out of the group is called *braiding* and is a key element in building the quantum computer – with its help we can construct

gates and operate the state. In case when the MZMs are bound to vortex cores, it can be realized when a vortex from one pair is adiabatically [9] moved around a vortex from the other pair at a large distance without ever approaching it. Each of the two selected MZMs can be seen as one fermionic mode with fixed parity $P_n = 1 - 2c_n^\dagger c_n \equiv i\gamma_{2n-1}\gamma_{2n}$. Despite the fact that the total parity $P_{\text{tot}} = \prod_n P_n$ is conserved, the parity of each pair can be changed during braiding, the procedure called *quantum state transfer.*

In order to have a fully functional quantum computer, we need to be able to generate arbitrary *n*-qubit unitary gate. However, not all the unitary operations can be performed using braiding [52, 53]. For the single-qubit operation we need the minimal set of 4 MZMs such that the qubit for the case of the odd total parity can be encoded depending on where does the fermion "sit": $|0\rangle \equiv |+\rangle |-\rangle , |0\rangle \equiv |-\rangle |+\rangle$[10] (see Fig. 1.3, panel a) for an example of implementation of the qubit on 4 MZMs bound to vortices). Exchange of two MZMs (also called "half-braid") corresponds to the square root of the Pauli matrices $\sqrt{\sigma_i}$ depending on which Majoranas are getting exchanged [14][11] (example of the implementation of $\sqrt{\sigma_x}$ can be seen on Fig. 1.3, panel c)). The latter correspond to the rotation of the qubit by $\pi/2$ with respect to the orthogonal axes on the Bloch sphere. It can be shown, that if we add a $\pi/4$ rotation around z-axis to out set of operations, a rotation by an arbitrary angle around any axis can be approximated with arbitrary accuracy [54]. However, that $\pi/4$ rotation which is also called T-gate can not be realized with braiding [14].

In order to construct any multi-qubit unitary operation, one needs a combination of a two-qubit gate (e.g CNOT that flips or not the state of the target qubit depending on the state of the control qubit) with single-qubit rotations [55]. The latter can be realized if we add the parity measurement that define the last step of the operation and the ancilla qubit [14] (see Fig. 1.4, left panel).

Braiding operation is very non-trivial and yet no one has succeeded in performing it. The MZMs bound to a defect or the end-point of a nanowire (as compared to the quantum Hall edge states) are immobile and therefore most proposals to demonstrate non-Abelian statistics generate the unitary braiding operation without physically moving the zero-modes in real space [20, 56–59]. Instead, the braiding is done in the parametric space. In the tri-junction

---

[9]The adiabaticity of the process is important to avoid Landau-Zener transitions.

[10]Equivalently, we could encode the qubit in the states $|-\rangle |-\rangle , |+\rangle |+\rangle$ if the total parity is even.

[11]For $\sqrt{\sigma_x}$ corresponds to the exchange of Majorana 2 and 3, $\sqrt{\sigma_y}$ - to the exchange of Majorana 1 and 3 and $\sqrt{\sigma_z}$ - to the exchange of Majorana 1 and 2.
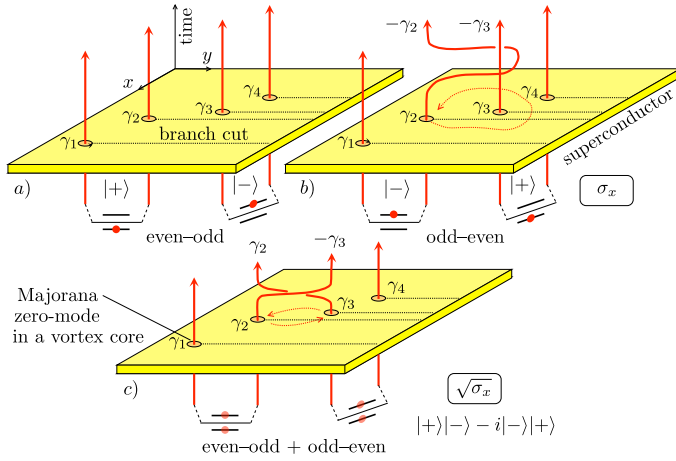
Figure 1.3. Panel a): a qubit $|0\rangle \equiv |+\rangle |-\rangle$, $|0\rangle \equiv |-\rangle |+\rangle$ built out of the four Majorana zero modes bound to vortices. Panel b) and c): operations σ_x, $\sqrt{\sigma_x}$ respectively performed by exchanging the vortices. *The figure is reprinted with permission from Beenakker, C. W. J, SciPost Phys. Lect. Notes, 2020*
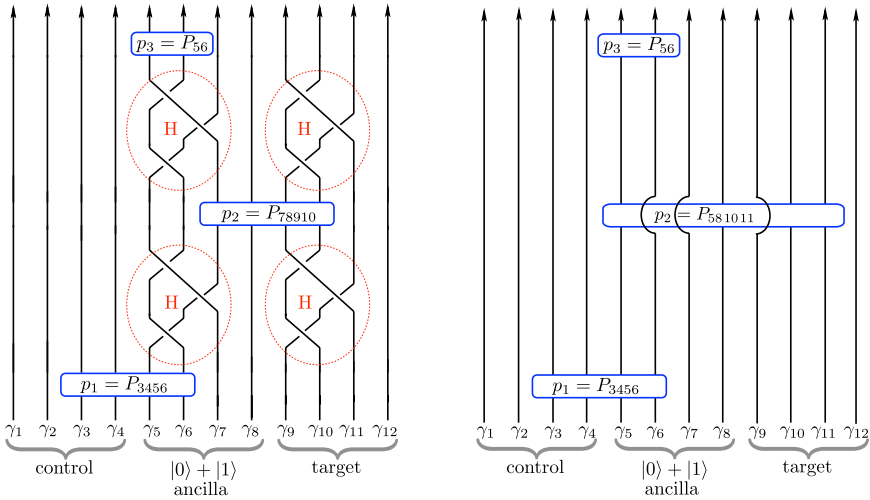

Figure 1.4. Two-qubit CNOT gate realized through braiding (left) and solely realized by projective parity measurements. *The figure is reprinted with permission from Beenakker, C. W. J, SciPost Phys. Lect. Notes, 2020*

introduced by by Alicea et al. [20] by varying the couplings between Majotanas $H(t) = \sum_{i=1}^{3} \Delta_i(t) i \gamma_0 \gamma_i$ and can transfer a Majorana zero-mode is transferred

from one end point to another (see Fig. 1.5). On practice, this can be either done by the electrostatic control using gate voltage [60] or by magnetic control tuning the magnetic flux through the Josephson junctions (see Fig 1.6) [57]. The advantage of the latter over the former is in the fact that the charge-sensitivity can be switched on and off with exponential accuracy by varying the magnetic flux through a split Josephson junction [61]. This gives us a macroscopic handle on the interaction of pairs of Majorana fermions.
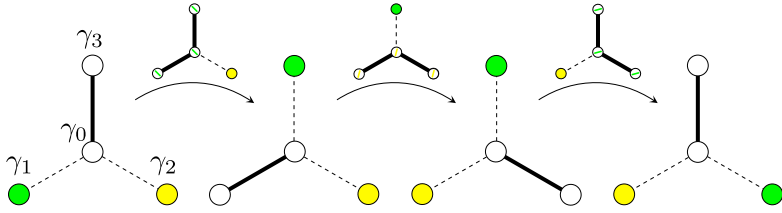

Figure 1.5. Braiding of Majorana zero modes (γ_1 and γ_2 in tri-junction.) γ_0 is an effective zero mode created when three MZMs got coupled in the middle of the tri-junction. To perform the braiding operation, one varies the couplings between the MZMs, thick lines denoting coupled Majoranas while dashed lines - decoupled. *The figure is reprinted with permission from Beenakker, C. W. J, SciPost Phys. Lect. Notes, 2020*
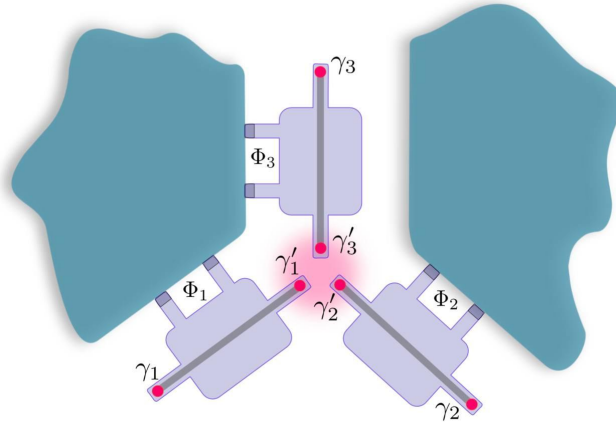

Figure 1.6. Three Cooper pair boxes with two Majorana zero-modes in each (pink dots). The three overlapping Majorana zero-modes that meet at the center of the at the tri-junction split to produce two no-zero levels and a single zero-mode. The coupling between the Majoranas in each Cooper pair box γ_i, γ_i' is varied by varying the flux Φ_i through the corresponding Josephson junction.

An arguably easier operation as compared to braiding appears to be able to completely substitute it [56]. This operation is a projective measurement called *fusion*. Physically, it is realized by bringing the vortices together so that the wave-functions of the zero-modes overlap. As a result, they split energetically, allowing to measure the fermion parity. The outcome of such a measurement is specified by the fusion rules. If we prepare the qubit in the state where γ_1, γ_2 and γ_3, γ_4 form states with definite fermion parity, the ground state degeneracy of the whole system will manifest itself in the non-deterministic outcome for the parity of the state formed from γ_2, γ_3. It follows from the anti-commutation relation for MZM which leads to $\langle P_{23} \rangle = \langle P_{12}P_{23}P_{12} \rangle = -\langle P_{12}P_{12}P_{23} \rangle = -\langle P_{23} \rangle$ In a formal notation the fusion rule is expressed by

$$\gamma_2 \times \gamma_3 = 1 + \psi, \tag{1.10}$$

where ψ indicates the presence of an unpaired fermion and 1 – no unpaired fermions [14]. Since the fusion rule 1.10 is a manifestation of the degenerate ground state and we know that the latter implies non-Abelian exchange statistic, one can conclude that the observation of the corresponding fusion rule is sufficient to announce the indirect demonstration of non-Abelian statistics.
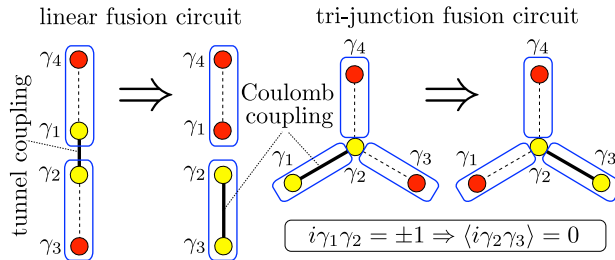

Figure 1.7. Two geometries to detect the fusion rule. *The figure is reprinted with permission from Beenakker, C. W. J, SciPost Phys. Lect. Notes, 2020*

Two easiest geometries to detect the fusion rule are presented on Fig. 1.7. In both geometries we perform a sequence of coupling and decoupling of the MZMs between each other. The difference between the linear and tri-junction is only in the mechanism of tuning the coupling (flux-controlled in the latter while in the former we have flux-controlled coupling inside the island and gate-controlled coupling between the islands). the sequence of steps is following [60]:

1. Start by coupling γ_1 and γ_2 performing the projective parity measurement P_{12} such that we effectively have one superconducting nanowire. The ground state is fixed by the total parity.

2. Decouple γ_1 and γ_2 and couple γ_2 and γ_3. The parity P_{23} is expected by have equal probability to be ± 1.

To experimentally perform a projective measurement on practice, one needs an observable that couples to it. The possible measurement schemes are:

- Majorana interferometry [58]. One brings the superconducting nanowire with MZMs into a weak contact with the normal metal and measures the current passing through it. The switches in parity result in parity-dependent Aharonov-Bohm oscillations in the magnetoconductance.

- Inductive coupling to a flux qubit [62]. The topological one-dimensional wire gets closed into circle by broken superconducting ring [63]. The section of the wire bridging the break of the superconducting ring remains nontopological and acts as a weak link (Josephson junction) between the two topological regions. Measuring the Josephson supercurrent can probe the 4π Josephson effect [17].

- Microwave coupling to a transmon qubit[12]. The nanowire with MZMs is incorporated into the Cooper pair box, the effective low energy Hamiltonian of which gets the term that depends on the parity of the nanowire [57]. The Cooper pair box is then placed in a microwave transmission line resonator changing its resonance frequency depending on the parity of the MZMs in the Cooper pair box [64].

- Capacitive coupling to a quantum dot. The superconducting nanowire is coupled to semiconductor quantum dots modulating the charge on them depending on the fermion parity of the zero-modes. The charge of the semiconductor quantum dots is then read-out capacitively [59, 65].

- If one wants to make a scalable read-out circuit performing a joint parity measurement on arbitrary pairs of Majorana zero-modes, one has to use Random Access Majorana Memory (RAMM) [66].

Bonderson, Freedman,and Nayak [56] showed how braiding of two MZMs (e.g γ_1 and γ_2 as on Fig. 1.5) can be performed through the sequence of projective measurements $\Pi_{kl} = \frac{1}{2}(1 + P_{kl})$ (Fig. 1.8). The idea is to project the state onto the state with definite parity (e.g +1). This can be done by measuring the parity and disregarding all the instances when it was equal

---

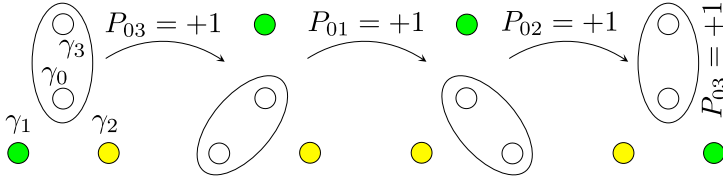[12]The transmon is a type of superconducting charge qubit

Figure 1.8. Braiding of Majorana zero modes (γ_1 and γ_2 in tri-junction.) γ_0 is an effective zero mode created when three MZMs got coupled in the middle of the tri-junction. To perform the braiding operation, one performs a sequence of projective measurements $P_{kl} = i\gamma_k\gamma_l$. The operations proceed only in case $P_{kl} = +1$, otherwise we need to start over. *The figure is reprinted with permission from Beenakker, C. W. J, SciPost Phys. Lect. Notes, 2020*

to -1. In this case, if we initialize the system in the state of even fermion parity and then we subsequently make sure that the parities P_{03} and then $P_{01}, \ldots, P_{03}$ is equal to $+1$ then due to the total parity conservation Majorana 1 must have been transferred to Majorana 3. The two-qubit operation CNOT can be also fully realized using projective measurements of parity.

It looks convincing that projective parity measurement is an important ingredient both in showing the non-Abelian statistic of the MZMs and for actually building a fault-tolerant quantum computer. As we have discussed in section 1.3.3, however, for the generic system that can host topologically protected MZMs, namely for a topological superconductors there exist parasitic low lying states (Andreev levels) that can contribute to the observables. The density of states of a "dirty" topological superconductor has a peak near zero energies, in Chapters 2 and 3 we have studied what influence these states can have one the measurement of the fusion rule.

1.5   Chaotic Majorana fermions

The Majorana zero modes that appear in the topological superconductors are non-interacting. The different point of view that considers the extreme case of strongly-correlated Majorana zero-modes can be studied and it appears to have many interesting and peculiar properties.

The SYK model was introduced by Kitaev [25] as a follow-up on the original disordered quantum Heisenberg model by Sachdev and Ye [26]. It contains $N \gg 1$ Majorana fermions in $0+1$ dimensions, with the Hamiltonian consisting

of a sum of all possible 4-fermion terms with random matrix elements

$$H = \frac{1}{4!} \sum_{i,j,k,l=1}^{N} J_{ijkl} \gamma_i \gamma_j \gamma_k \gamma_l, \tag{1.11}$$

where γ_i are Majorana zero modes, the couplings J_{ijkl} are drawn independently from Gaussian distribution with zero mean $\overline{J_{ijkl}} = 0$ and finite variance $\overline{J_{ijkl}^2} = 3!J^2/N^3$. The parameter J regulates the degree on entanglement in the system and by varying it we can enter phases with different qualitative behaviour of the system (we will elaborate on it later).

One can make two generalizations of this model:

1. Consider q-fermion interactions instead of 4-fermion as in 1.11 [31]. However, it appears that the non-trivial behaviour of the system shows up already for $q = 4$ therefore we will proceed with this "minimal" case further on in this thesis.

2. One can write the same model for complex fermions instead of real Majorana fermions (so-called cSYK) described by the Hamiltonian[13].

$$H_{\text{SYK}} = \frac{1}{(2N)^{3/2}} \sum_{i,j,k,l=1}^{N} J_{ij;kl} c_i^\dagger c_j^\dagger c_k c_l, \tag{1.12}$$

where again $J_{ij;kl} = J_{kl;ij}^*$ is a standard complex normal random variable with zero mean and variance J^2.

The SYK model drew the attention to itself due to a list of peculiar properties such as saturating the upper bound on quantum chaos [28] which is also the case for holographic duals of black hole horizons [29] and the absence of the well defined quasi-particles in strong coupling limit ($J/T \gg 1$). Let us elaborate on it a bit.

The degree to which the system is chaotic of the system is usually formulated in terms of the so-called Out-Of-Time-Order-Correlation function (OTOC) introduced by Larkin and Ovchinnikov [67].

$$C(t) \equiv -\langle [W(t), V(0)]^2 \rangle \tag{1.13}$$

where $\langle \ldots \rangle$ represents the thermal average. A naive understanding of the connection between the OTOC and chaos can be seen from the following

---

[13]The features of the SYK model mentioned in this section are valid for both models with real (Majorana) and complex fermions

consideration. Take $W(t) = x(t)$ be the position operator and $V(t) = p(t)$ the momentum operator in a quantum system. Then, in the semiclassical limit we replace the commutator $[x(t), p(0)]$ in the OTOC by the Poisson bracket $\{x(t), p(0)\} = \delta x(t)/\delta x(0)$. For a classically chaotic system, the latter would grow exponentially in time with the so-called Lyapunov exponent λ: $\delta x(t)/\delta x(0) \sim e^{\lambda t}$.

It was recently shown by Maldacena, Shenker, and Stanford [28] that in the many-body quantum system OTOC can not grow faster then exponentially with a characteristic time-scale $t_L \leq \hbar/(2\pi k_B T)$ which is correspondingly called Lyapunov time. It was also shown that in SYK OTOC behaves exactly in this way: it has the exponential growth with the precisely saturates the upper bound on the Lyapunov time [28].[14]

Another peculiar property of the SYK model is the power-law behaviour of the spectral function in the low energy region $\omega \ll J$. Meanwhile, the absence of long-living quasiparticles in high-temperature superconducting materials above the critical temperature is an immutable characteristic of the so-called strange metal state. Strange metals also exhibit a power-law behavior in the spectral function similarly to SYK. A lack of quasiparticles manifests itself in fast equilibration at low temperature on a timescale set by the Planckian relaxation time $t_P = \hbar/(2\pi k_B T)$ that is the same timescale that appears as an upper bound on quantum chaos. The extensions of this model to the cSYK coupled clusters predict thermal diffusivity [68] $\propto t_P$ and reproduce the linear in temperature resistivity, [69] observed in strange metals. [70, 71] Recently, a proposed theory of a Planckian metal, [27] based on the destruction of a Fermi surface by the cSYK-like interactions, shows that the universal scattering time equals the Planckian time t_P. The latter one characterizes the linear in temperature resistivity property [72] and was detected in cuprates, [73] pnictides, [74] and twisted bilayer graphene, [75] regardless of their different microscopic nature.

1.5.1   Mean field solution for cSYK

The SYK model appears to be tractable in the limit when we have many flavours of the fermions $N \gg 1$ (so-called large N limit). Let us try to derive the solution in this limit and study it closer. To do so, let us calculate the

---

[14]For the quantum mechanical system, however, the OTOC does not grow eternally but saturates at the Ehrenfest time t_E (by which the wave function have spread over the whole system).

partition function of the cSYK model and look for the saddle-point solution (mean field approach).

We start with the Gaussian probability distribution for the complex variable $J_{ij;kl}$ with mean zero and variance $J^2/2$,

$$\mathcal{P}(J_{ij;kl}, J_{ij;kl}^*) = \frac{1}{\sqrt{2\pi J^2}} \exp\left(-\sum_{ij;kl} \frac{J_{ij;kl} J_{ij;kl}^*}{2J^2}\right) \qquad (1.14)$$

In the limit $N \to \infty$ we can calculate the averaged [15] partition function accounting for the constraints $J_{ij;kl}^* = J_{kl;ij}$ and the symmetry under $i \leftrightarrow j$ and $k \leftrightarrow l$

$$Z = \int \mathcal{D}[c, c^\dagger] \int dJ_{ij;kl} dJ_{ij;kl}^* \delta(J_{ij;kl}^* - J_{kl;ij}) \delta(J_{ij;kl} + J_{ji;kl}) \delta(J_{ij;kl} + J_{ij;lk}) \times$$

$$\times \mathcal{P}(J_{ij;kl}, J_{ij;kl}^*) \exp\left(iS[c, c^\dagger]\right) \qquad (1.15)$$

where later on we will denote $\delta(J_{ij;kl}^* - J_{kl;ij}) \delta(J_{ij;kl} + J_{ji;kl}) \delta(J_{ij;kl} + J_{ij;lk}) = \delta(J)$.

Kadanoff-Baym equations

When we are in the non-equilibrium case we have to employ the Schwinger-Keldysh formalism. The action is

$$S[c, c^\dagger] = \sum_{s=\pm} \int dt \left(is \sum_i c_{is}^\dagger \partial_t c_{is} - \frac{s}{(2N)^{3/2}} \sum_{ij;kl=1}^N J_{ij;kl} c_{is}^\dagger c_{js}^\dagger c_{ks} c_{ls}\right), \quad (1.16)$$

where $s = \pm$ denotes forward and backward branches of the Keldysh time contour [76].

Disorder average will boil down to calculation of the following integral where we re-scaled $J_{ij;kl} \to J_{ij;kl}/\sqrt{2}J$

$$I = \int dJ_{ij;kl} dJ_{ij;kl}^* \frac{\delta(J)}{\sqrt{\pi}} e^{-\sum_{ij;kl}\left(J_{ij;kl} J_{kl;ij} + i \sum_{s=\pm} \frac{s\sqrt{2}J}{(2N)^{3/2}} \int dt J_{ij;kl} c_{is}^\dagger c_{js}^\dagger c_{ks} c_{ls}\right)}$$

$$(1.17)$$

---

[15] For many quantities, the model is self-averaging, and computing with some randomly chosen, but fixed, couplings should give the same result as averaging over the couplings. We also assume that there is no replica symmetry breaking.

We decompose the SYK part into two

$$\sum_{ij;kl} J_{ij;kl} c_{is}^\dagger c_{js}^\dagger c_{ks} c_{ls} = \frac{1}{2} \sum_{ij;kl} \left(J_{ij;kl} c_{is}^\dagger c_{js}^\dagger c_{ks} c_{ls} + J_{ij;kl}^* c_{ls}^\dagger c_{ks}^\dagger c_{js} c_{is} \right) \quad (1.18)$$

Then one can see that

$$\sum_{ij;kl} \left(J_{ij;kl} + \frac{iJ}{\sqrt{2}(2N)^{3/2}} \int dt \sum_{s=\pm} s c_{ls}^\dagger c_{ks}^\dagger c_{js} c_{is} \right) \times$$

$$\times \left(J_{ij;kl}^* + \frac{iJ}{\sqrt{2}(2N)^{3/2}} \int dt \sum_{s=\pm} s c_{is}^\dagger c_{js}^\dagger c_{ks} c_{ls} \right) =$$

$$= \sum_{ij;kl} \left(J_{ij;kl} J_{ij;kl}^* + i \sum_{s=\pm} \frac{s\sqrt{2}J}{(2N)^{3/2}} \int dt J_{ij;kl} c_{is}^\dagger c_{js}^\dagger c_{ks} c_{ls} - \right.$$

$$\left. - \frac{J^2}{2(2N)^3} \sum_{s,s'=\pm} ss' \int dt \int dt' c_{ls}^\dagger c_{ks}^\dagger c_{js} c_{is} c_{is'}^\dagger c_{js'}^\dagger c_{ks'} c_{ls'} \right)$$

$$(1.19)$$

One can integrate over the $J_{ij;kl}^*$ using the delta-function and shift the constant

$$J_{ij;kl} \rightarrow J_{ij;kl} + \frac{iJ}{\sqrt{2}(2N)^{3/2}} \int dt \sum_{s=\pm} s c_{ls}^\dagger c_{ks}^\dagger c_{js} c_{is}$$

and obtain

$$I = \int dJ_{ij;kl} \delta(J_{ij;kl} + J_{ji;kl}) \delta(J_{ij;kl} + J_{ij;lk}) \frac{1}{\sqrt{\pi}} \exp\left(-\sum_{ij;kl} J_{ij;kl} J_{kl;ij} \right) \times$$

$$\times \exp\left(-\sum_{ij;kl} \frac{J^2}{2(2N)^3} \sum_{s,s'=\pm} ss' \int dt \int dt' c_{ls}^\dagger c_{ks}^\dagger c_{js} c_s c_{is'}^\dagger c_{js'}^\dagger c_{ks'} c_{ls'} \right) \quad (1.20)$$

Note that now we do not have the condition $J_{ij;kl}^* = J_{kl;ij}$. Therefore

$$I = K(J) e^{-\sum_{ij;kl} \frac{J^2}{2(2N)^3} \sum_{s,s'=\pm} ss' \int dt \int dt' c_{ls}^\dagger c_{ks}^\dagger c_{js} c_s c_{is'}^\dagger c_{js'}^\dagger c_{ks'} c_{ls'}} \quad (1.21)$$

which gives the following partition function

$$Z = K(J) \int \mathcal{D}[c, c^\dagger] \exp\left(-\sum_{s=\pm} s \int dt \sum_i c_{is}^\dagger \partial_t c_{is} - \right.$$

$$\left. - \sum_{ij;kl} \frac{J^2}{2(2N)^3} \sum_{s,s'=\pm} ss' \int dt dt' c_{ls}^\dagger c_{ks}^\dagger c_{js} c_s c_{is'}^\dagger c_{js'}^\dagger c_{ks'} c_{ls'} \right) \quad (1.22)$$

Introducing bilocals $G_{s,s'}(t,t') = iN^{-1}\sum_i c^\dagger_{is'}(t')c_{is}(t)$ we arrive at effective action written with $\Sigma_{ss'}(t,t')$, $\Pi_{ss'}(t,t')$ as the corresponding Lagrange multipliers

$$S = -iN\mathrm{tr}\ln\Big[\sigma^z_{ss'}\delta(t-t')\,(i\partial_t+\mu)-\Sigma_{ss'}(t,t')\Big]-$$

$$-iN\sum_{ss'}\int dt dt'\Big(\Sigma_{ss'}(t,t')G_{s's}(t',t)-\frac{ss'J^2}{4}G_{ss'}(t,t')^2 G_{s's}(t',t)^2\Big)$$

In the large N limit, the saddle-point equations are

$$\Sigma_{ss'}(t,t') = J^2 G_{ss'}(t,t')^2 G_{s's}(t',t) \tag{1.23}$$

$$\sum_r \int_{-\infty}^{+\infty} du\Big(\sigma^z_{sr}\delta(t-u)\,(i\partial_t+\mu)-sr\,\Sigma_{sr}(t,u)\Big)G_{rs'}(u,t') = \delta_{ss'}\delta(t-t').$$

Schwinger-Dyson equations

The same kind of analysis with disorder averaging can be applied for the equilibrium case at some temperature T using Matsubara formalism. The imaginary time action averaged over disorder is

$$S = \int_0^\beta d\tau\Big[\sum_{i=1}^N \bar{c}_i\partial_\tau c_i + \int_0^\beta d\tau'\frac{J^2}{4N^3}\sum_{i,j,k,l=1}^N \bar{c}_i\bar{c}_j c_k c_l(\tau)\bar{c}_l\bar{c}_k c_j c_i(\tau')\Big], \tag{1.24}$$

where β is the inverse temperature. Same as for non-equilibrium, we make Hubbard-Stratonovich transformation introducing bilocals
$G(\tau,\tau') = -N^{-1}\sum_{i=1}^N c_i(\tau)\bar{c}_i(\tau')$ together with $\Sigma(\tau,\tau')$ as the corresponding Lagrange multipliers we get:

$$S = -N\sum_{n=-\infty}^{+\infty}\log\Big[i\omega_n-\Sigma_c(i\omega_n)\Big]-$$

$$-\int_0^\beta d\tau\int_0^\beta d\tau'\Big[N\Big(\Sigma_c(\tau,\tau')G_c(\tau',\tau)+\frac{J^2}{4}G_c(\tau,\tau')^4\Big)\Big], \tag{1.25}$$

where $\omega_n = \pi(2n+1)/\beta$ are Matsubara frequencies. In the limit of $N\gg 1$, the saddle-point equations are:

$$\Sigma(\tau) = J^2 G(\tau)^3$$

$$G(i\omega_n)^{-1} = i\omega_n - \Sigma(i\omega_n), \tag{1.26}$$

where $\omega_n = \pi T(2n+1)$ are Matsubara frequencies.

Emergent conformal symmetry

In the long time limit $1 \ll J\tau \ll N$, we can neglect the term with the derivative ∂_t and the theory becomes invariant under the re-scaling of the time $\tau \to f(\tau)$. The Kadanoff-Baym equations reduce to

$$- J^2 \sum_r sr \int_{-\infty}^{\infty} du G_{sr}(t, u)^2 G_{rs}(u, t) G_{rs'}(u, t') = \delta_{ss'}\delta(t - t') \qquad (1.27)$$

with the solutions

$$G_{ss}(t) = -i\,\mathrm{sign}(t) \cdot s \cdot \frac{e^{-is\pi/4}}{\sqrt{\sinh(\pi|t|/\beta)}},$$
$$G_{ss'}(t) = -is' \cdot \frac{e^{-i\mathrm{sign}(t)s'\pi/4}}{\sqrt{\sinh(\pi|t|/\beta)}} \qquad (1.28)$$

with $b = \pi^{1/4}/\sqrt{2\beta J}$.

For Matsubara formalism we get

$$G(\tau) = \frac{b}{\sqrt{\tau}}\mathrm{sign}(\tau). \qquad (1.29)$$

1.5.2   SYK in the lab

We see that seemingly simple and somewhat solvable SYK model shares many phenomena intrinsic to the mysterious strongly correlated systems that do not yet have a clear theoretical description. It inspired several proposals to realize the SYK model in a condensed matter platform in the lab [22, 23, 77–79]. For the corresponding realistic systems, SYK is expected to arise as a low-energy effective description.

Let us take a closer look into one of the mentioned proposals. Chen et. al. [77] propose a to take a graphene flake with irregular boundary in the external magnetic field (see Fig. 1.9. The spectrum of graphene in a perpendicular magnetic field B consists of quantized Landau levels $E_n \simeq \hbar v \sqrt{2n(eB/\hbar c)}$. The chiral symmetry of graphene protects the 0th Landau level from the presence of disorder. Therefore, if we project on the low energy sector, we get a highly degenerate subspace[16] with the wave functions $\Phi_i(\mathbf{r})$ being random in space thanks to the disordered boundary. The SYK model arises as the

---

[16]The degeneracy of the 0th Landau level is proportional to the flux of the magnetic field through the flake

effective model for the low energy sector when Coulomb repulsion $V(\mathbf{r} - \mathbf{r}')$[17] is added into the consideration. The the corresponding interaction matrix elements between the zero modes are given by

$$J_{ij;kl} = \int d\mathbf{r} \int d\mathbf{r}' \Phi_i^*(\mathbf{r}) \Phi_j^*(\mathbf{r}') V(\mathbf{r} - \mathbf{r}') \Phi_k(\mathbf{r}) \Phi_l(\mathbf{r}'). \tag{1.30}$$

Thanks to the randomness in the spatial distribution of $\Phi(\mathbf{r})$ the distribution of the coupling constants $J_{ij;kl}$ can be approximated by the Gaussian to an arguably good extend (see Fig. 1.9, right panel). The effective Hamiltonian is therefore of the form of the complex SYK model (cSYK) 1.12.
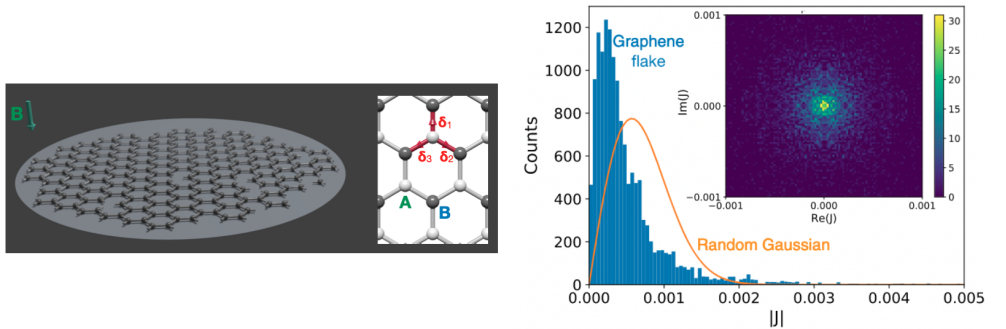

Figure 1.9. Left panel: Schematic depiction of the proposed design of the experimental simulation of the cSYK model. Graphene flake with the irregular boundary in the external perpendicular magnetic field. Inset: lattice structure of graphene. Right panel: Histogram of the coupling constants $|J_{ij;kl}|$ from Eq. 1.30 for $N = 16$ compared to the Gaussian distribution (orange line) with the same variance. *The figure is reprinted with permission from Anffany Chen, R. Ilan, F. de Juan, D. I. Pikulin, and M. Franz, Phys. Rev. Lett. 121, 036403, (2018)*

However, after building the setup it is good to check whether the system that we prepared in the lab is actually close enough to the SYK and if it possesses the same fundamental properties e.g. whether it is in the non-Fermi liquid phase. There are many reasons why it may not be so, for example: the wave-function of the ground state is not random enough such that the effective coupling strength $J_{ij;kl}$ do not follow the Gaussian distribution or the microscopic parameters are not tuned such that we are not in the strong coupling regime $J/T \gg 1$. Also, it is known, that adding even an infinitesimal quadratic term (simple hopping) to the SYK model can destroy its non-trivial

---

[17]The screened Coulomb potential is $V(\mathbf{r}) = (e^2/\varepsilon r)e^{-r/\lambda}$ with ε being the dielectric constant and λ - Thomas-Fermi length.

transform it to free random fermions (Fermi liquid phase) [80]. And probing the experimental setup that is allegedly described by the SYK model would mean coupling it by tunneling to a fermion bath in one way or another. In Chapters 4 and 5 we study several possible observable signatures of the non-Fermi liquid phase in the SYK as well as the robustness of this phase when we couple the SYK to a fermion bath.

1.6   Cosmic Majorana fermions

One more place where we can meet Majorana fermions (in form of fundamental particles) is neutrino physics. When Ettore Majorana was writing his famous equation, he was surely inspired by the particles that were introduces seven years prior by Pauli. Despite the fact that these particles are not yet fully understood theoretically (for example, the value of the masses and its mechanism), they are not in any sense rare, quite the opposite – we are being surrounded by them. In fact, there are approximately as many neutrinos flying around us as there are photons, order of hundred in every cm^3!

In fact, the analogy with the photons goes further – there is a radiation background similar to the Cosmic Microwave Background (CMB) that is correspondingly called Cosmic Neutrino Background or CνB. The mechanism of both is the same: the very early universe was filled with the relativistic particles that scatter between one another. As the universe was expanding approximately at the moment when the rate of the scattering processes because equal to the Hubbard parameter the corresponding particles decoupled – the Universe because transparent for them. Starting from that moment they were penetrating the universe moving (almost) freely. Such particles are called relic and by detecting them we are able to look into the early universe. CMB is a "photograph" of relic photons that were decoupled when the Universe was hundred thousands years old. The same cold, $T = 1.95\,\mathrm{K}$, radiation for neutrinos that decoupled much earlier then photons (when the Universe was only living for seconds) is called Cosmic Neutrino Background (CνB) [81].

Despite many similarities, CνB and CMB have a drastic difference – neutrinos are much harder to detect. Indirect evidence for the existence of the relic neutrinos was found in the observed CMB [82], however, due to the extreme weakness of the interactions between neutrinos and other forms of matter, direct detection of the CνB remains a major experimental challenge.

Today it is widely accepted that the most practicable route to the direct detection of the CνB lies through the measurement of the fine structure of the
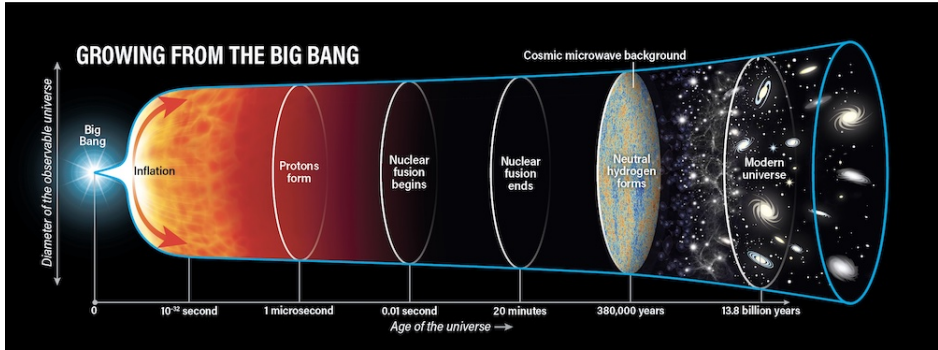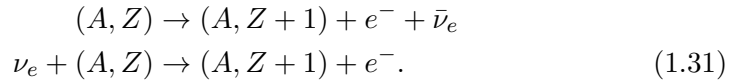
Figure 1.10. Schematic depiction of the expanding Universe after the Big Bang. *The picture taken from Astronomy: Roen Kelly, after BICEP2 Collaboration*

β-spectrum of a radioactive element [83–87]. Let us consider a general case of nuclear β-decay and neutrino capture

$$(A, Z) \to (A, Z + 1) + e^- + \bar{\nu}_e$$
$$\nu_e + (A, Z) \to (A, Z + 1) + e^-. \tag{1.31}$$

The processes of capture of cosmic neutrino having mass m_ν by a sample of radioactive atoms characterized by the beta-decay energy Q are predicted to leave a potentially discernible signature in the form of an extremely faint peak at the energy $Q + m_\nu^0 c^2$ in the beta spectrum of the sample [83–87] (see Fig. 1.11) [18]. On the other hand, the major part of the spectrum of the radioactive element consists of the events of the spontaneous β decay and forms a continuum with the upper cut-off energy $Q - m_\nu^0 c^2$. Therefore, one expects the neutrino capture peak to be separated from the end of the spontaneous β-spectrum by an energy gap of at least one neutrino mass and for that reason to be discernible at least in principle.

From the first glance, it is obvious why such an experiment can be very challenging: we are trying to measure a meV [19] feature on the background of keV. This requires extreme energy resolution (order of $10\,\text{meV}$). However, another major challenge lies in the weakness of the signal. A naive estimate for the neutrino capture cross section is $\sigma_\nu \simeq (\tau Q)^{-1}$ [86], where $Q \sim 10\,\text{keV}$ is the energy released in the β-decay and τ is the lifetime of the β emitter.

---

[18]There are, generally, three mass generations of neutrino. This fact does not influence our considerations so we will omit it further. Here m_ν^0 is a mass of the lightest neutrino.

[19]The best up to date bound on the effective neutrino mass is $m_\nu < 0.8\,\text{eV}$ as obtained by the KATRIN experiment using gaseous molecular tritium [89].
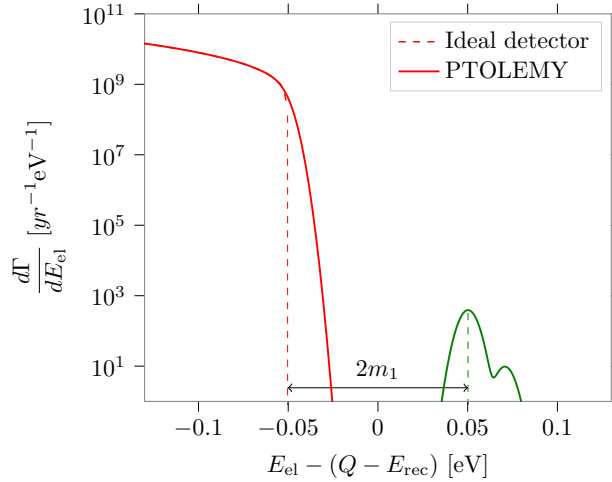
Figure 1.11. he β-spectrum of free monoatomic Tritium centered around $Q - E_{\text{rec}}$, where Q is the decay energy and E_{rec} - recoil of the nucleus in the vacuum. The normal neutrino mass hierarchy [88] is assumed with the mass of the lightest neutrino $m_1 = 50$ meV. The spontaneous β-decay spectrum is shown in red while the CνB feature is shown in green. The solid lines are drawn assuming a 10 meV resolution of the detector.

We have a lower bound on the lifetime (otherwise we would not be able to assemble the experimental setup) $\tau \gtrsim 1$yr and also all the viable emitters have $Q \sim 10$ keV. Therefore, we arrive at the conclusion that in order to have at least one neutrino capture event per year we need large amounts of the radioactive atoms (at least 100 g in order to achieve one event per year in the case of atomic Tritium).

The lower bound on the size of the experimental setup comes from a very simple consideration – it should be bigger then the mean free path of the emitted electron with respect to the hard core collisions with the other emitters. Otherwise, the scattering processes will corrupt the energy resolution. The mean free path is given by the cross section $\sigma = R_{\text{atom}}^2$ and the concentration of the emitters $n = N/L^3$. The number of the emitters is fixed $N \sim 10^{23}$ from the requirements of sufficient activity, the radius of the atom is also known. If we calculate the numbers, we would see that the very rough estimate of the lower bound on the linear size of the experimental setup is of the order of 1 km. The biggest relic neutrino detector nowadays is KATRIN that has the cross- section area of the container about 50 cm^2, so the effective mass of

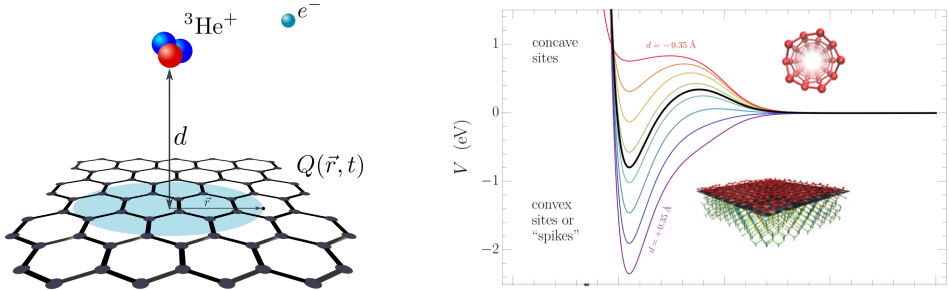tritium molecules is only about $50\,\mu g$ [90].

Figure 1.12. Left panel: Schematic depiction of the decaying Tritium atom attached to the graphene sheet. Right panel: Graphene–hydrogen binding potential as a function of the distance from the binding site. Different colors correspond to different local curvatures (puckering) of the binding site. Flat graphene corresponds to $d = 0$ (thick black line), while $d > 0$ corresponds to convex sites and $d < 0$ to concave ones.

The only viable solution to the problem of the controllable handling of such a large amount of radioactive material nowadays is proposed by the PTOLEMY collaboration [85]. It is based on the idea to use a sold state-based experimental architecture. In this proposal, the tritium atoms are deposited on the graphene substrate which can efficiently store atomic tritium by locally binding it to carbon atoms (either by chemisorption, physisorption). Along with the high tritium storage, PTOLEMY also offers a very precise control over the emitted electrons with the help of the elaborate configuration of the electric and magnetic fields that "guide" the electrons to the detector. An overall energy resolution of $10\,\text{meV}$ is achieved.

1.6.1 β decay on the surface

As was first pointed out [91], the coupling of the β-emitter to the many-body solid state system comes at the price of introducing additional intrinsic energy uncertainty to the β spectrum. Indeed, when we are interested in the processes on as low energy scales as meV, the solid state substrate becomes a jungle filled with many-body phenomena.

In order to understand how the spectrum will look for the β-decaying atom bounded to the substrate, let us apply the Fermi Golden Rule to the whole system containing β-decaying constituents and the substrate. Let us denote the total state of such a system (atom + environment) as $|\alpha, z\rangle$. Since the whole system is closed, the Fermi Golden Rule holds where the total energy

is conserved.

$$\Gamma = \frac{2\pi}{\hbar} \sum_{\text{final states}} |\langle \text{final}| \, \hat{H}^\beta \, |\text{initial}\rangle \, |^2 \delta \left(E_{\text{in}} - E_{\text{fin}} \right), \qquad (1.32)$$

where we know that the initial and final states have different number of protons and neutrons that is why only the Hamiltonian of the weak interaction H^β survives. Let us specify how initial and final states look like and what are their quantum numbers

$$
\begin{aligned}
|\text{initial}\rangle &= |\alpha_0, z\rangle \\
|\text{final}\rangle &= |\alpha, z+1\rangle \, |k\rangle \, |p\rangle \,,
\end{aligned}
\qquad (1.33)
$$

where there are 3 quantum numbers: an abstract label for the atom together with the environment state α, electron momentum k and neutrino momentum p[20].

The Hamiltonian density of the β-interaction in the full generality is

$$H^\beta = \frac{G_\beta}{\sqrt{2}} \bar{e}(x) \gamma^\mu (1 - \gamma_5) \nu_e(x) \hat{J}^{\text{nucl}}_\mu(x) + \text{h.c}, \qquad (1.34)$$

where $e(x), \nu_e(x)$ are electron and neutrino fields and $\hat{J}^{\text{nucl}}_\mu(x)$ is a nuclear part which depends on the atom itself and we do not specify it. We get

$$\Gamma = \frac{V^2}{\hbar} \int \frac{d^3k d^3p}{(2\pi)^6} \sum_\alpha |\langle k| \, \langle p| \, \langle \alpha, z+1| \, H^\beta \, |\alpha_0, z\rangle \, |^2 \int d\tau e^{i\tau(E_e + E_\nu - E_{\alpha_0} + E_\alpha)},$$
$$(1.35)$$

where we used that $\delta(E_{\text{in}} - E_{\text{fin}}) = \int \frac{d\tau}{2\pi} e^{i\tau(E_e + E_\nu - E_{\alpha_0} + E_\alpha)}$. Expanding $| \cdot |^2$ we get

$$
\begin{aligned}
\Gamma = \frac{1}{\hbar} \int \frac{d^3k d^3p}{(2\pi)^6} \int dx dx' j^\mu_{\text{lept}}(x, \vec{p}, \vec{k}) j^{*,\nu}_{\text{lept}}(x', \vec{p}, \vec{k}) \times \\
\times \sum_\alpha \langle \alpha_0, z| \, \hat{J}^{\text{nucl}}_\mu(x) \, |\alpha, z+1\rangle \, \langle \alpha, z+1| \, \hat{J}^{\dagger,\text{nucl}}_\nu(x') \, |\alpha_0, z\rangle \times \\
\times \int d\tau e^{i\tau(E_e + E_\nu + E_\alpha - E_{\alpha_0})}, \qquad (1.36)
\end{aligned}
$$

---

[20]We note that in this we neglect the Coulomb interaction of the emitted electron with the nucleus and with the surroundings. Therefore, the emitted electron is a plane wave that is characterized by the momentum k. Neutrino does not interact with anything so it is generally a plane wave (specified by the momentum p).

where $j_{\text{lept}}^{\mu}(x, \vec{p}, \vec{k}) = \bar{\psi}_e(x, \vec{k})\gamma^{\mu}(1 - \gamma_5)\psi_{\nu}^c(x, \vec{p})$ and ψ has both functional dependence (plane wave e^{ipx} without normalization factor as we already took it into account) and spinor structure. Accounting for

$$\sum_{\alpha} e^{i\tau E_{\alpha}} |\alpha, z+1\rangle \langle\alpha, z+1| = e^{i\tau \hat{H}_{z+1}^{\alpha}}, \qquad (1.37)$$

where $\hat{H}^{\alpha, z+1}$ is the Hamiltonian that describes the system that consists of the isotope of the initial atom with the charge $z+1$ and environment, we get[21]

$$\Gamma = \frac{1}{\hbar} \int \frac{d^3k d^3p}{(2\pi)^6} \Big| \int dx\, j_{\text{lept}}^{\mu}(x, \vec{p}, \vec{k}) J_{\mu}^{\text{nucl}}(x) \Big|^2 \times$$

$$\times \int d\tau \, \langle\alpha_0, z| \hat{\chi}^{\dagger} e^{i\tau \hat{H}_{z+1}^{\alpha}} \hat{\chi} |\alpha_0, z\rangle \, e^{i\tau(E_e + E_{\nu} - E_{\alpha_0})}, \qquad (1.38)$$

where $\hat{\chi}$ changes the charge of the nucleus by one and $|\alpha, z\rangle$ only has the information about the surroundings and the electron orbitals of the atom, not the nucleus itself, the latter is in $J^{\text{nucl}}(x)$. Denoting

$$\frac{1}{2\pi} \int d\tau \, \langle\alpha_0, z| \hat{\chi} e^{i\tau \hat{H}_{z+1}^{\alpha}} \hat{\chi}^{\dagger} |\alpha_0, z\rangle \, e^{i\tau\omega} = \mathcal{F}(\omega), \qquad (1.39)$$

we get the generalized Fermi Golden rule that accounts for the interactions of the nucleus with the surroundings

$$\Gamma = \frac{1}{\hbar} \int \frac{d^3k d^3p}{(2\pi)^6} \Big| \int dx\, j_{\text{lept}}^{\mu}(x, \vec{p}, \vec{k}) J_{\mu}^{\text{nucl}}(x) \Big|^2 \mathcal{F}(E_e + E_{\nu} - E_{\alpha_0}). \qquad (1.40)$$

Or

$$\frac{d\Gamma}{dE_e} = \frac{4E_e p(E_e)}{(2\pi)^4 \hbar} \int E_{\nu} k(E_{\nu}) dE_{\nu} \times$$

$$\times \Big| \int dx\, j_{\text{lept}}^{\mu}(x, E_e, E_{\nu}) J_{\mu}^{\text{nucl}}(x) \Big|^2 \mathcal{F}(E_e + E_{\nu} - E_{\alpha_0}). \qquad (1.41)$$

If we compare it with the Fermi Golden Rule for the β-decay in the vacuum

---

[21] With the assumption that the wave function of the atom is a product of the wave function of the nucleus and the wave function of the electron shells that only depends on the charge of the nucleus.

$$\frac{d\Gamma^{(0)}}{dE_e} = \frac{4E_e p(E_e)}{(2\pi)^4 \hbar} \int E_\nu k(E_\nu) dE_\nu \times$$
$$\times \left| \int dx j^\mu_{\text{lept}}(x, E_e, E_\nu) J^{\text{nucl}}_\mu(x) \right|^2 \delta(E_e + E_\nu - E_{\alpha_0}). \qquad (1.42)$$

We see that the presence of the substrate leads to the finite lifetime of the daughter atom (that is encoded in the function $\mathcal{F}(\omega)$). This leads to the broadening of the β-spectrum. It includes all the types of the interactions of the emitter with the substrate. Among them (the list is not by any means exhaustive):

1. Zero-point motion of the emitter [91].

2. Finite lifetime of the daughter ion due to redistribution of the charges on its shells and tunneling to graphene.

3. Breakdown of the angular momentum conservation due to the presence of the substrate.

4. Sudden emission of an electron from a beta-decayer leaves behind a positively charged centre which attracts the electric current carriers in of the substrate. This effect results in what is known as the X-ray edge anomaly - a gamma-shaped broadening of the emission peak [92].

5. Creation of vibrational excitations of the lattice.

6. Emission of plasmons and surface polaritons.

7. Inhomogeneous broadening due to any kind of inhomogeneities in the emitter arrangement.

However, the spectrum described by Eq. 1.40 does not include the interaction of the emitted electron with the substrate that can also manifest itself through many different mechanisms such as

1. Screening of the daughter atom by the charges in graphene.

2. Creation of shock wave emission due to the motion of the emitted electron at grazing angles at speeds exceeding the Fermi velocity.

3. Etc.

The investigation of one of the points in this list, namely the zero-point motion of the emitter (Chapter 6) rules out the Tritium-on graphene design and calls for substantially heavier beta-decayers. As is described in Chapter 7, it was found [93] that the best candidates in terms of the suppression of zero-point motion (also accounting for other criteria such as long enough lifetimes, stable daughter nucleus, single β decay branch, etc.) are ^{171}Tm and ^{151}Sm. These isotopes have lower neutrino capture cross sections as compared to Tritium: ≈ 50 times smaller for ^{171}Tm and 3 orders of magnitude lower for ^{151}Sm[93].

Some aspects of the electric effects of the interaction of the emitted electron with the substrate are considered in Chapter 8 and it seems that they are much less dangerous as compared to the effects due to interaction of the β-emitter with the substrate. Naively, this can be motivated by the fact that the emitted electron near the edge of the spectrum has quite high velocity $v \approx 0.3c$. Therefore it leaves the system pretty fast and does not "notice" many effects that take place on longer timescales.

To conclude, the research in the condensed matter side of this experimental setup is only starting, many effect have not yet been investigated. Before building a full scale experiment, both theoretical and, especially, experimental programs in condensed matter physics and surface science are required to study quantum devices with a mono-layer of rare earth elements (such as Thulium) attached to graphene substrate.

1.7 This thesis

This thesis aims to touch several questions about Majoranas of various origin:

1. For Majorana modes in superconductor. In the systems of the symmetry class D (to which topological superconductors belong) Majorana zero modes at zero energy can be mimicked by Andreev levels.

   Can the vanishing fermion parity in the superconductor fusion experiment be taken as a distinctive signature of the isolated Majorana modes? If not, what would be the alternative scenario that would allow to discriminate true degenerate ground state against the accidental degeneracies of Andreev levels?

2. What signatures of the non-Fermi liquid phase can we see by probing the SYK model by the means of transport and beyond?

3. It is known, that adding even an infinitesimal quadratic term (simple hopping) to the SYK model can destroy its non-trivial transform it to free random fermions (Fermi liquid phase) [80]. So, if we want to probe the SYK experimentally by the means of transport, it would inevitable mean coupling it to the some kind of lead. We want to know whether there is some domain of stability of the non-Fermi liquid phase of SYK under such a perturbation.

4. The last question that is considered in this thesis is very practical. We want to know what limitation do the many-body effects in the experimental device impose on the energy resolution of the whole set-up. In particular, it concerns the experiment of the relic neutrino detection. It is still unclear whether the neutrino is a Majorana particle or not and what is the absolute scale of its masses [94]. Along with answering on this question, relic neutrino detection will allow us to look in the very early universe (much earlier then the Cosmic Microwave Background allows us to see). Such an experiment is therefore of fundamental importance. The state of the art proposal for it requires big amount of the source material (order of 10^{23} of heavy radioactive elements) and an extreme energy resolutions (order of $10\,\mathrm{meV}$) [85]. It is widely accepted that the only way to have a chance to full fill such requirements is to used a solid state based experimental device which again brings us to the interplay of high energy physics and low energy phenomena.

Below, I briefly highlight the main results presented in the thesis.

1.7.1   Chapter 2

Kitaev's Pfaffian formula equates the ground-state fermion parity of a closed system to the sign of the Pfaffian of the Hamiltonian in the Majorana basis. Using Klich's theory of counting statistics for paired fermions we generalize the Pfaffian formula to account for quantum fluctuations in the fermion parity of an open subsystem. A statistical description in the framework of random-matrix theory is used to answer the question when a vanishing fermion parity in a superconductor fusion experiment becomes a distinctive signature of an isolated Majorana zero-mode.

1.7.2   Chapter 3

Detection of the fusion rule of Majorana zero-modes is a near-term milestone on the road to topological quantum computation. An obstacle is that the non-deterministic fusion outcome of topological zero-modes can be mimicked by the merging of non-topological Andreev levels. To distinguish these two scenarios, we search for dynamical signatures of the ground-state degeneracy that is the defining property of non-Abelian anyons. By adiabatically traversing parameter space along two different pathways one can identify ground-state degeneracies from the breakdown of adiabaticity. We show that the approach can discriminate against accidental degeneracies of Andreev levels.

1.7.3   Chapter 4

The Planckian relaxation rate $\hbar/t_\mathrm{P} = 2\pi k_\mathrm{B} T$ sets a characteristic timescale for both the equilibration of quantum critical systems and maximal quantum chaos. In this note, we show that at the critical coupling between a superconducting dot and the complex Sachdev-Ye-Kitaev model, known to be maximally chaotic, the pairing gap Δ behaves as $\eta\,\hbar/t_\mathrm{P}$ at low temperatures, where η is an order one constant. The lower critical temperature emerges with a further increase of the coupling strength so that the finite Δ domain is settled between the two critical temperatures.

1.7.4   Chapter 5

The Sachdev-Ye-Kitaev (SYK) model describes interacting fermionic zero modes in zero spatial dimensions, *e.g.* quantum dot, with interactions strong enough to completely washout quasiparticle excitations in the infrared. In this paper, we consider the complex-valued SYK model at initial temperature T and

chemical potential μ coupled to a large reservoir by a quench at time $t = 0$. The reservoir is kept at zero temperature and charge neutrality. We find that the dynamics of the discharging process of the SYK quantum dot reveals a distinctive characteristic of the SYK non-Fermi liquid (nFl) state. In particular, we focus on the tunneling current induced by the quench. We show that the temperature dependent contribution to the current's half-life scales linearly in T at low temperatures for the SYK nFl state, while for the Fermi liquid it scales as T^2.

1.7.5   Chapter 6

Beta-spectrum of radioactive atoms was long ago predicted to bear an imprint of the Cosmic Neutrino Background (CνB) [95]. Over the years, it has been recognised that the best chance of achieving the signal-to-noise ratio required for the observation of this effect lies with solid-state designs [96]. Here we bring to the fore a fundamental quantum limitation on the type of beta-decayer that can be used in a such a design. We derive a simple usability criterion and show that ^{3}H, which is the most popular choice, fails to meet it. We provide a list of potentially suitable isotopes and discuss why their use in CνB detection requires further research.

1.7.6   Chapter 7

Recent analysis of the viability of solid state-based relic neutrino detectors has revealed the fundamental necessity for the use of heavy, $A > 100$, β-decayers as neutrino targets. Of all heavy isotopes, ^{171}Tm and ^{151}Sm stand out for their sufficiently low decay energies, reasonable half-life times and stable daughter nuclei. However, the crucial bit of information, that is the soft neutrino capture cross-section is missing for both isotopes. The main reason for that is a particular type of β-decay, which precludes a simple link between the isotope's half-life time and the neutrino capture rate. Here we propose an experimental method to bypass this difficulty and obtain the capture cross-section of a soft neutrino by a given isotope from the isotope's β-spectrum.

1.7.7   Chapter 8

The only promising experimental architecture for the Cosmic Neutrino Background (CνB) detection nowadays exploits β-decay of the emitters bounded to a solid state substrate. The artifact of such a design is the appearance

of the additional intrinsic bounds on the energy resolution coming from the various types of interactions of the β-decaying atom with the collective modes in the substrate. In this work, we only focus on the electromagnetic effects, namely: 1) charge relaxation of the electrons in the substrate as a response to the ionization of the β emitter, 2) electron-hole pairs creation by the emitted β electron.